Multimodal, label-free nonlinear optical imaging for applications in biology and biomedical science

Research article

Journal of RAMAN SPECTROSCOPY

Received: 18 March 2013 Accepted: 20 March 2013 Published online in Wiley Online Library: 11 June 2013

(wileyonlinelibrary.com) DOI 10.1002/jrs.4305

Multimodal, label-free nonlinear optical imaging for applications in biology and biomedical science†

R. Mouras,[a]* P. Bagnaninchi,[b] A. Downes[a] and A. Elfick[a]

We have developed a multimodal optical platform for label-free imaging on the basis of nonlinear optical microscopy (NLO) for applications in biology and biomedical science. Three application areas have been chosen as examples: regenerative medicine, drug delivery monitoring and cancer diagnosis. Obtained data showed the potential of NLO microscopy for the following: (1) investigating the stem cell differentiation states prior their use in regenerative medicine and tissue repair, (2) tracking drug molecules in living cells and (3) detecting cancer by imaging biopsies *ex vivo*. The results of this study illustrate the potential to translate NLO microscopy from *ex vivo* to *in vivo* applications. Copyright © 2013 John Wiley & Sons, Ltd.

Supporting information may be found in the online version of this article.

Keywords: multimodal microscopy; multiphoton microscopy; CARS microscopy; label-free imaging; drug delivery monitoring; cancer diagnosis; stem cells

Introduction

For decades, microscopy has been a key tool in the investigation of biological processes, imaging of cellular structures and the localisation of molecules within cells. The identification of different molecular species on the microscopic scale is still a considerable challenge in many areas of biology. Fluorescence microscopy is a key research tool in biomedical science, enabling cells and tissues to be imaged in three dimensions and localise specific molecules of interest. However, this technique, as powerful as it is, has a number of significant limitations, which cause significant barriers: (1) photobleaching of fluorophores, which makes continuous observation of biochemical processes difficult; (2) cells have to be genetically modified to express fluorescence, or exogenous fluorescent labels are added, both of which may cause perturbation of the system of interest and are time-consuming; and (3) experiments are often performed on fixed samples preventing the study of dynamic processes. There is a real need to develop non-invasive techniques dedicated to real-time imaging.

Spontaneous Raman microscopy is a non-invasive technique, which probes a molecule's intrinsic vibrational modes[1]. Detecting the vibrational signatures of molecules circumvents the need for fluorescent or other extrinsic tags and permits the visualisation of the distribution of specific molecules (chemically selective imaging) with high sensitivity.

Recently, Raman microscopy has been used to image living cells, by adapting a different approach by illuminating a line and collecting a set of spectra from all points along this line, in parallel, rather than taking a Raman spectrum at each pixel.[2,3] Unfortunately, despite the efforts performed to develop Raman microscopy, low signal levels limit this technique; hence, either a large number of molecules or long acquisition times are required, presenting significant limitations to the development of real-time studies.

Over the past decade, new microscopy approaches using coherent Raman scattering as a contrast mechanism have been emerged as powerful techniques to address these limitations. Coherent anti-Stokes Raman scattering (CARS) microscopy[4–10] is an established resonant Raman technique, where the molecular vibrations are driven coherently through stimulated excitation by pulsed lasers. The CARS signal is greatly amplified, around five orders of magnitude over traditional Raman spectroscopy, offering new possibilities for high sensitive detection in living cells and tissue, with high chemical specificity and inherent three-dimensional (3-D) optical sectioning capability.[11–13]

In addition, complementary nonlinear optical (NLO) techniques, such as two-photon excitation fluorescence (TPEF), and second harmonic generation (SHG) have been widely used for biological specimens imaging [14–17]. TPEF exploits the autofluorescence of biological samples or added tags, and SHG makes use of the noncentrosymmetric properties to image structural proteins such as collagen[15] and myosin[18]. In combination with CARS, these modalities provide a wealth of chemical and biological information, which can help to resolve the most persistent biological questions. These techniques have the potential to revolutionise biomedical imaging offering the new insights into the biochemistry and pathways at the subcellular level[19,20].

* *Correspondence to: Rabah Mouras, Institute for Materials and Processes, School of Engineering, The University of Edinburgh, Edinburgh, EH9 3JL, UK E-mail: r.mouras@ed.ac.uk*

† *This article is from the ECONOS part of the joint special issue on the European Conference on Nonlinear Optical Spectroscopy (ECONOS 2012) with Guest Editors Johannes Kiefer and Peter Radi and the II Italian Conference of the National Group of Raman Spectroscopy and Non-Linear Effects (GISR 2012) with Guest Editor Maria Grazia Giorgini.*

a *Institute for Materials and Processes, School of Engineering, The University of Edinburgh, Edinburgh, EH9 3JL, UK*

b *MRC-Centre for Regenerative Medicine, The University of Edinburgh, Edinburgh, EH16 4SB, UK*

In this paper, we investigate the use of NLO in biomedical science as a label-free technique for real-time monitoring of chemotherapeutic drug action in living cells, for breast cancer tissue imaging and to monitor and quantify stem cell (SC) differentiation into the osteoblast (bone) and adipocyte (fat) lineages.

Experimental

Multimodal microscope

The experimental setup (Fig. 1) used in this study is described elsewhere.[21] Briefly, the pump (532 nm, 5 ps) was used to pump an optical parametric oscillator (Levante Emerald), and the Stokes (1064 nm, 6 ps) beams were generated by a mode-locked Nd: YVO_4 laser source (PicoTrain, High-Q laser). The Stokes and the output signal of the optical parametric oscillator were collinearly combined and focused on the sample using a 60× oil immersion objective (Plan Apo VC, NIKON) with 1.4 numerical aperture and directed into a confocal laser-scanning microscope. A laser-scanning confocal inverted optical microscope (Nikon BV 'C1', Amsterdam, Netherlands) is used to acquire images. The configuration of the system enables both backward (epi-) and forward detection schemes. An appropriate set of dichroic mirrors, short-pass and band-pass filters (Chroma, Rockingham, USA) are used to selectively transmit the desired NLO signals. Photomultiplier tubes (*R3896 Hamamatsu*) are used to acquire CARS, TPEF and SHG images simultaneously using a three-channel detection scheme. For the imaging of living cells and *in situ* observation of anticancer drug delivery, glass bottom dishes were used. All the imaging experiments were carried out at 22 °C for tissue samples or 37 °C for living cells. The temperature was controlled by means of a heating stage. The laser power at sample was 12 and 8 mW for the pump and Stokes beams, respectively. All images were 512 × 512 pixels, acquired by Nikon EZ-C1 3.4 software and processed using *ImageJ*. The lateral and depth resolution with a 60× oil immersion objective was measured to be 0.25 and 1.1 μm, respectively.[11]

Cell culture and tissue sections preparation

Cancer cells

Human rectal carcinoma H630 (chemosensitive) and their derived subclones resistant (chemoresistant) cells H630-RT cell lines were generously provided from the group of Prof. M. Frame group (Edinburgh Cancer Research UK Centre, ECRC) and cultured according to standard mammalian tissue culture protocols and sterile technique. The cell lines were cultured in RPMI 1640 medium supplemented with 10% foetal calf serum, 100 Units ml^{-1} penicillin and 100 μg ml^{-1} streptomycin. Cell lines were incubated at 37 °C in a humidified 5% CO_2-containing atmosphere. The chemoresistant cell lines H630-RT were generated *in vitro* by continuous exposure of the parent line to 5-Fluouracil (5FU). Over time, continuous exposure of 5FU-sensitive cells (H630) to 5FU caused the cells to become resilient to this treatment[22]. Finally, the chemoresistant cells were maintained in normal culture medium containing 10 μM of 5FU.

Stem cells

Human adipose-derived SCs (ADSCs) (Invitrogen) were expanded to passage three in a low serum medium (complete RS MesenPRO, Invitrogen) with 2 mM L-glutamine supplement according to the supplier protocol. ADSCs were induced after 93 h towards either osteoblast or adipocyte lineages with, respectively, an osteogenesis or an adipogenesis differentiation medium (Invitrogen). In two weeks post-induction, end point staining was performed to assess that ADSCs were induced towards osteoblasts using *Alizarin red staining* and towards adipocytes using oil-red-oil (data not shown).

All cell lines were cultured in glass bottom Petri dishes (Fluorodish Cell Culture Dish – 35 mm, World Precision Instruments) in a humidified incubator at 37 °C and 5% CO_2.

Tissue sections for microscopy

All tissue samples used in this study were donated anonymously by patients from the Edinburgh Royal Infirmary. Tissue sections were cut from paraffin-embedded blocks to a thickness of 10 μm using a microtome. Sections were mounted either on glass slides (SuperFrost Plus) that had been coated with an adhesion agent or on borosilicate cover slips for NLO microscopy measurements. Haematoxylin and eosin (H&E) staining was conducted for conventional histopathological observation. Finally, the tissue section was dewaxed using Histoclear deparaffinisation reagent.

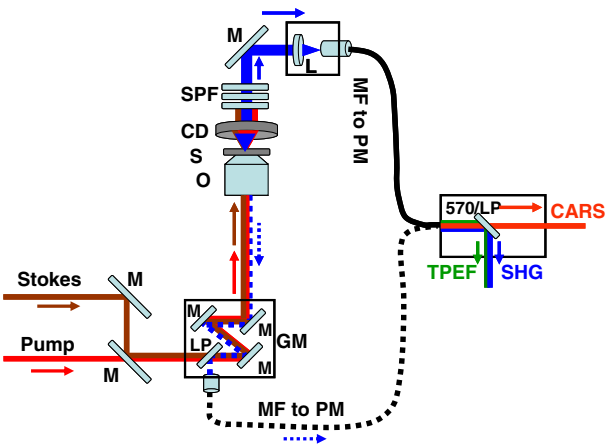

Figure 1. Schematic diagram of the multimodal microscope setup. M, mirror; LP, long pass dichroic mirror; GM, galvano mirrors; O, objective; S, sample; CD, condenser; SPF, short-pass filters set; L, focusing lens; MF, multimode fibre, PM; photomultiplier.

Results

CARS microscopy of live cells

The CARS microscopy is a powerful technique for minimally invasive live cell imaging without the need of any labelling, using only endogenous chemical contrast. However, the CARS images thus obtained are composed of contributions from both the resonant and the nonresonant (NR) signals, which limit the utility of CARS. To overcome this drawback, many techniques such as heterodyne CARS[23], frequency modulated CARS[24], Polarised CARS[25] and so on, were developed to suppress the NR signal.

Because the NR signal arises from the electronic structure of the molecule of interest and does not carry any chemically selective information, it can be visualised by tuning the excitation frequency away from that of the desired molecular vibration. Thus, a background-free image can be obtained by subtracting the NR image from the resonant image without altering the chemical information or distorting the image. Figure 2 depicts CARS images of wild-type breast cancer cells (MCF7-WT) obtained by tuning the Raman shift to the CH_2 stretch vibration in lipids on resonance at 2840 cm^{-1}, off resonance at 3050 cm^{-1} and the difference image (on-off). The obtained image is background-free, and the contrast

Journal of RAMAN SPECTROSCOPY

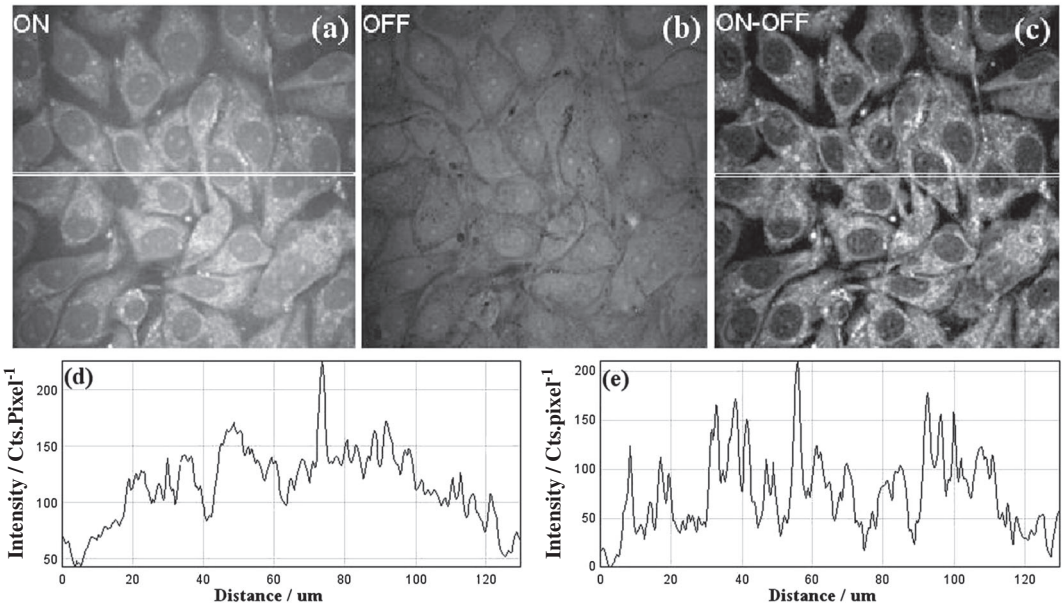

Figure 2. CARS images of wild-type breast cancer (MCF7-WT) live cells obtained at different frequencies. (a) On resonance wavenumber of CH_2 stretch vibration at 2840 cm^{-1}, (b) off resonance wavenumber at 3050 cm^{-1} and (c) the difference on-off. Image size (130 × 130 μm) and the acquisition time was 21 s per image. Signal-to-noise ratio is greatly enhanced as shown on the intensity profiles from (d) on resonance CARS image and (c) the difference on-off image.

is increased by a factor of ~3 as shown on the line profiles plotted in Fig. 2(d, e). All CARS images were acquired following this protocol. One can see that the nuclei are well resolved because of the chemical contrast between the cytoplasm, which contains huge amount of lipids, and the nuclei, which are mainly composed of DNA. This is of great interest for biologist as they always use staining by Hoechst in living cells or DAPI on fixed cells to visualise the nuclei.

Monitoring chemotherapeutic drugs using CARS and TPEF

The multimodality of our system allows us to acquire multiple images simultaneously. Hence, we can use CARS to image the cells, whereas TPEF can be used for the colocalisation of the drug molecules. In our study, we used doxorubicin (Dox) as a test molecule. This drug is autofluorescent, and it is known to intercalate into the DNA to retard replication, pushing the cells to undergo apoptosis[26] (programmed cell death). Thus, we used TPEF to investigate the intracellular distribution of Dox in chemosensitive cells and in their chemoresistant variants. The cells were incubated with 10 μM of Dox for 20 min and then transferred onto the multimodal microscope for imaging. First, we took CARS and TPEF images at $t = 20$ min (Fig. 3). To monitor the drug uptake in real time, we kept the cells under observation for 100 min, and TPEF images of Dox were taken every 5 min

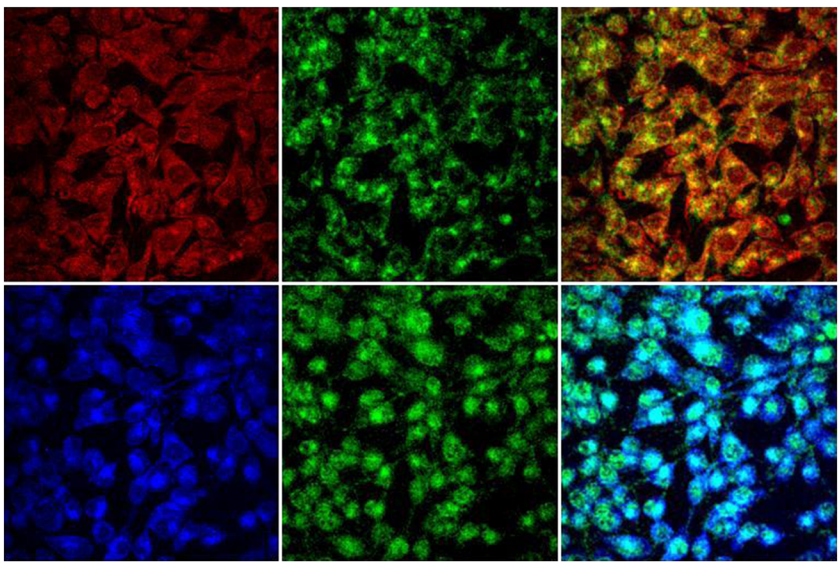

Figure 3. (150 × 150 μm) multimodal image showing the accumulation of doxorubicin in H630 chemosensitive cells at $t = 20$ min (upper panel) and at $t = 120$ min (lower panel) post-incubation with 10 μM of Dox. (Left): CARS images of H630 obtained at CH_2 stretch vibration wavenumber (2840 cm^{-1}) showing the morphology of the cells at the beginning and the end of the treatment, (centre): TPEF of Dox acquired using a band-pass filter at 580 nm and (right): overlay of CARS and TPEF images showing the localisation of Dox molecules within the cells. Images were taken at 3 μm inside the cells and with an accumulation time of 21 s per image.

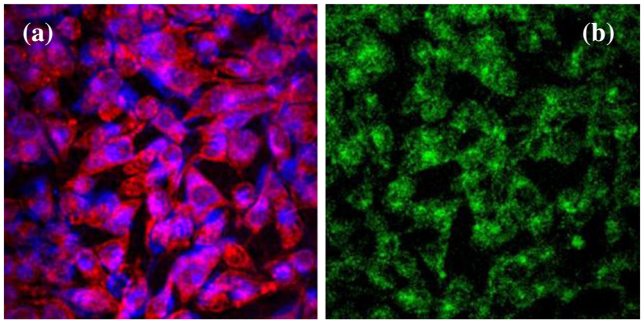

Figure 4. (a) comparison of CARS images at $t = 20$ min (Red) and $t = 120$ min (Blue) showing the morphology change of the cells because of the shrinkage of the cells under Dox effect. (b) Monitoring of Dox trafficking for 100 min. The movie (supporting information) is made of a total of 20 TPEF images taken every 5 min. Image size (150×150 μm) and accumulation time was 21 s per image. This figure is available in colour online at wileyonlinelibrary.com/journal/jrs

(20 images in total). The data obtained are presented as a movie in Fig. 4(b) (supporting information). After 2 h, we took both CARS and TPEF images and compared them with images taken at the beginning of the process. Figure 3 shows CARS/TPEF images of chemosensitive cells at the $t = 20$ min and $t = 120$ min. We can see clearly the accumulation of Dox in the cytoplasm and mainly in the nuclei. The accumulation of a high concentration of Dox in the nuclei implies the absence of any resistant mechanisms against Dox. We also found that Dox molecules reach the nuclei in less than 30 min, and the effect of drugs can be noticeable in a few hours. After 2 h of incubation with Dox, the chemosensitive cells show the early signs of their reaction to the drugs by shrinking and start to undergo apoptosis (Fig. 4(a)). These results show the efficacy of Dox on the chemosensitive cells.

However, in the resistant subclones, drug molecules appear to be located mainly in the cytoplasm in the nuclei periphery, and take up to 24 h to reach the nuclei and accumulate in high concentrations. This is due to the multidrug resistance developed by these cells, which are continuously cultured with 10 μM of 5FU (Fig. 5). Previous studies have shown that the presence P-glycoprotein on the plasma membrane is responsible of the development of multidrug resistance mechanisms and the influx of the drugs outside the cells[27,28].

The 3-D sectioning capability permits visualising the distribution of Dox within the cells. Figure 5(d) highlights the 3-D distribution of Dox in H630-RT cells. The image consists of Z-stack of ten images taken at 1 μm steps. The visualisation of the 3-D distribution of drug molecules shows that drugs are preferentially localised in the cytoplasm and completely absent in the nuclei. These observations demonstrated that Dox is differently distributed in the chemosensitive H630 and in their chemoresistant variants H630-RT.

Multimodal microscopy as a diagnostic tool for cancer: toward clinical application

The utilisation of fluorophores is not always possible because of their toxicity; hence, the focus of this research is to demonstrate alternative imaging modalities.[29–32] Systems that can use endogenous markers within the body are preferable, for example, redox measurements, SHG signals from collagen, TPEF from autofluorescent elastin, and then CARS for examining specific lipid or protein structures.

Figure 6 depicts a multimodal image of breast ductal carcinoma embedded in paraffin compared with its H&E staining and transmitted light. Note that all lipids were removed chemically with the paraffin during the dewaxing process. The multimodal image is rich in information that cannot be obtained from transmitted light or H&E staining. The CARS image at the CH_3 vibration wavenumber (2950 cm^{-1}) shows aggregations of cells lying within extracellular matrix.

The multimodal image illustrates the localisation of these protein structures within the fibrous–collagen network and elastin imaged by SHG and TPEF, respectively. The shape of these features indicates that these regions are solid tumours. These observations concur with those that may be drawn from the H&E stained sections, confirming the utility of NLO in this application. Furthermore, Fig. 6 illustrates additional advantages of multimodal imaging when compared with H&E staining. The high levels of SHG signal generated are associated with a highly ordered tissue; disorganised structures produce lower signal. This suggests that the observed fibrous tissue is predominantly constituted from collagen type I, as it has the crystalline and noncentrosymmetric properties required for generating high SHG signal[33]. This organised structure of collagen is in a good agreement with previous investigations showing the reorganisation of collagen fibres to facilitate the local invasion of tumour cells.[34] Likewise, 3-D information regarding the content, distribution and structure of collagen is easily accessible by adopting a multimodal approach. This valuable information is beneficial to understanding of the pathologic changes that occur in breast cancer and cannot be readily obtained using classical histolopathology techniques.

The results obtained demonstrate the usefulness of multimodality for understanding the distribution of the elastin–collagen network of the extracellular matrix in addition to the localisation of tumours, as

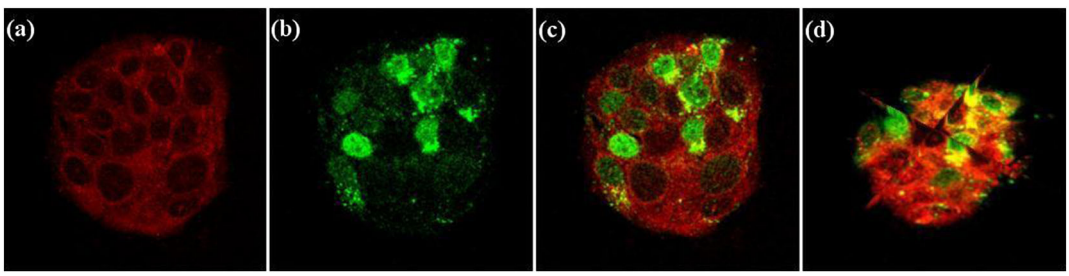

Figure 5. (130×130 μm) multimodal image showing the accumulation of doxorubicin in H630-RT chemoresistant cells after 24 h post-incubation with 10 μM of Dox. (a) CARS images of H630 obtained at CH_2 stretch vibration wavenumber (2840 cm^{-1}) showing the morphology of the cells, (b) TPEF of Dox acquired using a band-pass filter at 580 nm, (c) overlay CARS/TPEF showing the localisation of Dox molecules in the nuclei and in the cytoplasm and (d) 3-D distribution of Dox inside the cells. Images were taken at 3 μm inside the cells and with an acquisition of 21 s per image.

Journal of RAMAN SPECTROSCOPY

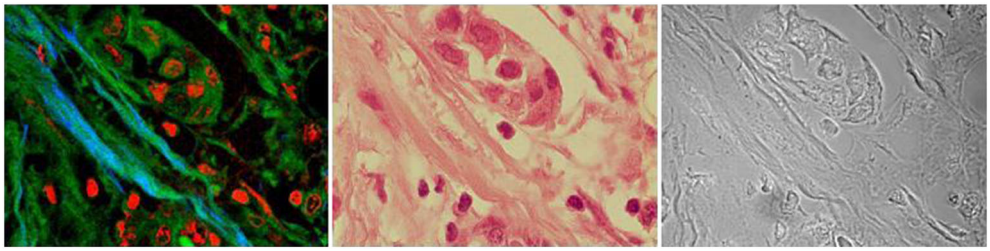

Figure 6. (Left): (100 × 75 μm) multimodal image of breast ductal carcinoma embedded in paraffin compared with its H&E staining (middle) and transmitted light (right). All lipids were removed chemically with the paraffin. CARS image obtained at CH_3 vibration wavenumber (2840 cm^{-1}) in proteins (red) highlighting the solid tumours lying in a connective tissue composed of fibrous collagen and elastin probed with SHG (blue) and TPEF (green), respectively. The time acquisition was 21 s per image. This figure is available in colour online at wileyonlinelibrary.com/journal/jrs

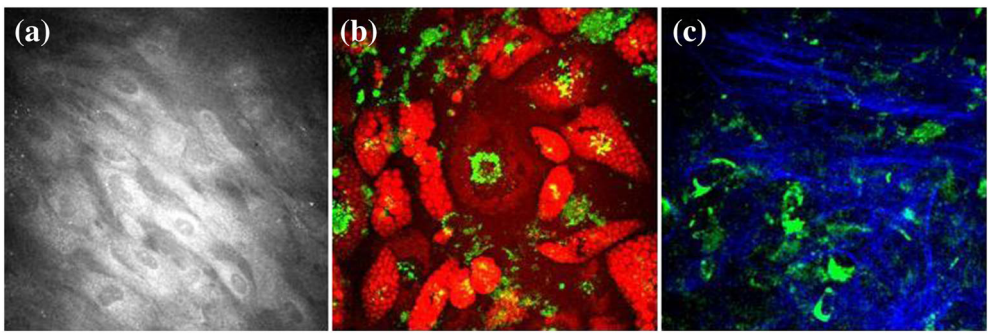

Figure 7. (212 × 212 μm) multimodal images of ADSC cells induced towards adipocytes and osteoblasts at day 14 post-induction showing changes in cell morphology and the appearance of functional markers such as lipid droplets (for adipocytes), fibrous collagen (osteopblasts) and FPs and lipofuscin. (a) CARS image of ADSCs control sample before induction obtained by probing the lipid stretch vibration wavenumber at 2840 cm^{-1}. (b) Overlay of CARS image (Red) of ADSC cells induced towards adipocytes obtained by probing the lipid stretch vibration wavenumber at 2840 cm^{-1} (red) showing the formation of lipid droplets around the nuclei, and TPEF (Green) of FPs and lipofuscin indicating the metabolic activity of the cells undergoing differentiation towards adipocyte. (c) Overlay of SHG of deposited fibrous collagen (blue) and TPEF of FPs and lipofuscin (green) in ADSCs induced towards osteoblasts. The acquisition time was 21 s for all images. This figure is available in colour online at wileyonlinelibrary.com/journal/jrs

well as their size and shape. These data show the ability of multimodal microscopy to be translated into clinical applications.

Multimodal microscopy applications in regenerative medicine: monitoring stem cells differentiation to different lineages

Adult SCs are likely candidates for cell therapy and for the study of *in vitro* disease models. In both cases, label-free assessment of the differentiated state of SCs is desirable either to prevent any harmful effects that could be caused by unwanted lineage or to facilitate time course studies of cell differentiation. We investigated NLO to monitor the differentiation of ADSCs into adipocytes and osteoblast lineages by using only inherent sources of contrast. The induction of ADSCs towards two different cell lineages was monitored in a non-invasive manner by using CARS, TPEF and SHG simultaneously at different time points.

Figure 7 displays multimodal images of ADSCs induced towards adipogenesis and osteogenesis after 14 days post-induction, compared with the negative control (noninduced cells).

Changes in cell morphology, together with the appearance of functional markers such as lipid droplet accumulation, and fibrous collagen matrix deposition for, respectively, adipo-induced and osteo-induced cells were observed. In addition, autofluorescent features appeared near the nuclei and in the endoplasmic reticulum. The spectral peak of TPEF of these features was found between 580 nm and 610 nm. Previous studies showed that these wavelengths correspond to the fluorescence of flavoproteins and lipofuscin.[35,36] The increase of the number of these features as well as their fluorescence signal during the differentiation process at different stages revealed that changes in cell metabolism were occurring throughout ADSC differentiation towards osteoblasts and adipocytes. These results show the potential of multimodal microscopy as an enabling technology to investigate SC differentiation, which is minimally invasive and is label-free.[37] CARS can be used to characterise the morphology of the cells undergoing differentiation, TPEF to monitor the metabolic activity by imaging the autofluorescence of flavoproteins, and SHG to investigate the fibrous collagen deposition. It is clear that the acquiring multiple image modes yield an enriched dataset with the ability to distinguish change in cell phenotype. It is probable that image processing, together with automated scanning, could enable the screening of SC-based *in vitro* models.

Conclusion

We have shown the potential of multimodal NLO microscopy for applications in biomedical science. By using only endogenous markers, we have been able to do the following: (1) monitor ADSCs differentiation towards two discrete lineages: adipogenesis and osteogenesis, (2) follow anticancer drugs in WT cells and their chemoresistant type subclones and (3) image tumours in breast tissue biopsies and observe their localisation within the extracellular matrix. The data obtained show that multimodal, multiphoton microscopy holds significant promise for the real-time imaging of drugs, cancer diagnosis and the non-invasive assessment of the

differentiation state of SCs prior to their use for cell therapy in regenerative medicine and tissue repair. Additionally, it opens the doors to biologists to observe multiple complex physiological and biochemical processes in real-time and in a cellular background that more closely reflects their natural environment, helping to address persistent biological questions without the need to use labels or perturbing approaches.

Supporting information

Supporting information may be found in the online version of this article.

References

[1] J. De Gelder, K. De Gussem, P. Vandenabeele, L. Moens, *J. Raman Spectrosc.* **2007**, *38*, 1133.
[2] K. Hamada, K. Fujita, N. I. Smith, M. Kobayashi, Y. Inouye, S. Kawata, *Proc. SPIE* **2007**, *6443*, 64430Z.
[3] Y. Harada, T. Ota, D. Ping, Y. Yamaoka, K. Hamada, K. Fujita, T. Takamatsu, *Proc. SPIE* **2008**, *6853*, 685308.
[4] M. D. Duncan, J. Reintjes, T. J. Manuccia, *Opt. Lett.* **1982**, *7*, 350.
[5] B. G. Saar, C. W. Freudiger, J. Reichman, C. M. Stanley, G. R. Holtom, X. S. Xie, *Science* **2010**, *330*, 1368.
[6] A. Volkmer, J. X. Cheng, X. S. Xie, *Phys. Rev. Lett.* **2001**, *87*, 023901.
[7] C. Heinrich, S. Bernet, M. Ritsch-Marte, *Appl. Phys. Lett.* **2004**, *84*, 816.
[8] J. Moger, B. D. Johnston, C. R. Tyler, *Opt. Express* **2008**, *16*, 3408.
[9] C. Krafft, A. A. Ramoji, C. Bielecki, N. Vogler, T. Meyer, D. Akimov, P. Rösch, M. Schmitt, B. Dietzek, I. Petersen, A. Stallmach, J. Popp, *J. Biophoton.* **2009**, *2*, 303–312.
[10] C. Y. Lin, J. L. Suhalim, C. L. Nien, M. D. Miljković, M. Diem, J. V. Jester, E. O. Potma, *J. Biomed. Opt.* **2011**, *16*, 021104.
[11] R. Mouras, G. Rischitor, A. Downes, D. Salter, A. Elfick, *J. Raman Spectrosc.* **2010**, *41*, 848.
[12] A. Zumbusch, G. Holtom, X. S. Xie, *Phys. Rev. Lett.* **1999**, *82*, 4142.
[13] A. Kachynski, A. Kuzmin, P. Prasad, I. Smalyukh, *Opt. Express* **2008**, *16*, 10617.
[14] W. Denk, J. H. Strickler, W. W. Webb, *Science* **1990**, *248*, 73.
[15] P. J. Campagnola, L. M. Loew, *Nat. Biotech.* **2003**, *21*, 1356.
[16] J. Mansfield, J. Yu, D. Attenburrow, J. Moger, U. Tirlapur, J. Urban, Z. Cui, P. Winlove, *J. Anat.* **2009**, *215*, 682.
[17] T. E. Matthews, J. W. Wilson, S. Degan, M. J. Simpson, J. Y. Jin, J. Y. Zhang, W. S. Warren, *Biomed. Opt. Expr.* **2011**, *2*, 1576.
[18] V. Nucciottia, C. Stringarib, L. Sacconib, F. Vanzib, L. Fusia, M. Linaria, G. Piazzesia, V. Lombardia, F. S. Pavone, *PNAS* **2010**, *107*, 7763.
[19] A. Downes, R. Mouras, P. Bagnaninchi, A. Elfick, *J. Raman Spectrosc.* **2011**, *42*, 1864.
[20] C. L. Evans, X. S. Xie, *Annu. Rev. Anal. Chem.* **2008**, *1*, 883.
[21] A. Downes, R. Mouras, A. Elfick, *J. Raman. Spectrosc.* **2009**, *40*, 757.
[22] L. Murray, The role of E-cadherin in colon cancer drug resistance, PhD thesis, http://theses.gla.ac.uk/1943/, University of Glasgow, **2010**.
[23] F. Lu, W. Zheng, Z. Huanga, *App. Phys. Lett.* **2008**, *92*, 123901.
[24] F. Ganikhanov, C. L. Evans, G. G. Saar, X. S. Xie, *Optics Lett.* **2006**, *31*, 1872.
[25] J. X. Cheng, L. D. Book, X. S. Xie, *Opt. Lett.* **2001**, *26*, 1341.
[26] F. A. Fornari, J. K. Randolph, J. C. Yalowich, M. K. Ritke, D. A. Gewirtz, *Mol. Pharmacol.* **1994**, *45*, 649.
[27] N. Baldini, K. Scotlandi, M. Serra, S. Toshiharu, N. Zini, A. Ognibene, S. Santi, R. Ferracini, N. M. Maraldi, *Eur. J. Cell Biol.* **1995**, *68*, 226.
[28] G. Wurzer, Z. Herceg, J. Wesierska-Gadek, *Cancer Res.* **2000**, *60*, 4238.
[29] R. Mouras, A. Downes, G. Rischitor, M. Mari, A. Elfick, *Proc. SPIE* **2010**, *7569*, 756933.
[30] H.W. Wang, L. L. Thuc, J. X. Cheng, *Opt. Comm.* **2008**, *281*, *1813*.
[31] H. Chen, H. Wang, M. N. Slipchenko, Y. Jung, Y. Shi, J. Zhu, K. K. Buhman, J.-X. Cheng, *Opt. Express* **2009**, *17*, 1282.
[32] R. S. Lim, A. Kratzer, N. P. Barry, S. Miyazaki-Anzai, M. Miyazaki, W. W. Mantulin, M. Levi, E. O. Potma, B. J. Tromberg, *J. Lip. Res.* **2010**, *51*, 1729.
[33] T. Hompland, A. Erikson, M. Lindgren, T. Lindmo, C. de Lange Davies, *J. Biomed. Opt.* **2008**, *13*, 054050.
[34] P. P. Provenzano, K. W. Eliceiri, J. M. Campbell, D. R. Inman, J. G. White, P. J. Keely, *BMC Med.* **2006**, *4*, 38.
[35] W. L. Rice, D. L. Kaplan, I. Georgakoudi, *PLoS One* **2010**, *5*, e10075.
[36] W. L. Rice, D. L. Kaplan, I. Georgakoudi, *J. Biomed. Opt.* **2007**, *12*, 060504.
[37] R. Mouras, P. Bagnaninchi, A. Downes, A. Elfick, *J. Biomed. Opt.* **2012**, *17*(11), 116011.